Biochimica et Biophysica Acta 1847 (2015) 1055–1063

Contents lists available at ScienceDirect

Biochimica et Biophysica Acta

journal homepage: www.elsevier.com/locate/bbabio

Reductive activation of *E. coli* respiratory nitrate reductase

Pierre Ceccaldi [a], Julia Rendon [a], Christophe Léger [a], René Toci [b], Bruno Guigliarelli [a], Axel Magalon [b], Stéphane Grimaldi [a], Vincent Fourmond [a,*]

[a] Aix-Marseille Université, CNRS, BIP UMR 7281, 31 chemin J. Aiguier, F-13402 Marseille cedex 20, France
[b] Aix-Marseille Université, CNRS, LCB UMR 7283, 31 chemin J. Aiguier, F-13402 Marseille cedex 20, France

ARTICLE INFO

Article history:
Received 9 April 2015
Received in revised form 1 June 2015
Accepted 7 June 2015
Available online 11 June 2015

Keywords:
Protein film voltammetry
EPR spectroscopy
Mo/W *bis*PGD enzyme family
Respiratory nitrate reductase

ABSTRACT

Over the past decades, a number of authors have reported the presence of inactive species in as-prepared samples of members of the Mo/W-*bis*PGD enzyme family. This greatly complicated the spectroscopic studies of these enzymes, since it is impossible to discriminate between active and inactive species on the basis of the spectroscopic signatures alone. *Escherichia coli* nitrate reductase A (NarGHI) is a member of the Mo/W-*bis*PGD family that allows anaerobic respiration using nitrate as terminal electron acceptor. Here, using protein film voltammetry on NarGH films, we show that the enzyme is purified in a functionally heterogeneous form that contains between 20 and 40% of inactive species that activate the first time they are reduced. This activation proceeds in two steps: a non-redox reversible reaction followed by an irreversible reduction. By carefully correlating electrochemical and EPR spectroscopic data, we show that neither the two major Mo(V) signals nor those of the two FeS clusters that are the closest to the Mo center are associated with the two inactive species. We also conclusively exclude the possibility that the major "low-pH" and "high-pH" Mo(V) EPR signatures correspond to species in acid–base equilibrium.

1. Introduction

Mo/W-*bis*PGD enzymes are ubiquitous enzymes characterized by an active site in which a Mo (or W) ion is ligated by the dithiolenes of two molybdopterin moeties [1,2]. Their oligomeric structures vary greatly, with enzymes that contain only the Mo/W active site and others that host a number of iron–sulfur clusters, hemes and/or other cofactors. They catalyze a variety of reactions, mostly two-proton, two-electron redox reactions, often coupled to the transfer of oxo groups. They can process a large range of substrates, and play fundamental roles in the bioenergetic metabolism of many prokaryotes. The metal ion (Mo or W) at the active site is thought to cycle between the IV, V and VI oxidation states during the course of the catalysis. Among other techniques, researchers have therefore used EPR spectroscopy to obtain information on the mechanism of these enzymes, as the intermediates Mo(V) or W(V) are EPR-active. However, this technique is not always conclusive. Indeed, a large number of Mo(V) signatures were identified on the different members of the Mo/W-*bis*PGD enzyme family [3], and sometimes many signatures on a single member (see Ref. [4] for an example of this diversity for the case of periplasmic nitrate reductases), but spectroscopy alone cannot tell whether a signature belongs to an intermediate in the catalytic cycle or if it arises from an inactive species. Indeed, it has been shown that some of the members of the Mo/W-*bis*PGD enzyme family are purified in an inactive form, such as the soluble DMSO reductase [5]. This raises the possibility that some of the signatures are those of inactive species, and indeed, some of us showed that this is the case for the periplasmic reductase NapAB from *Rhodobacter sphaeroides* (*Rs*), for which the major Mo(V) signature is that of an inactive species that activates upon reduction [6,7].

Respiratory nitrate reductases (Nar) are membrane-bound members of the Mo/W-*bis*PGD enzyme family that catalyze the reduction of nitrate to nitrite coupled to the oxidation of quinols, leading to the generation of a protonmotive force. They have been purified and characterized from different organisms: *Escherichia coli* (*Ec*) [8], *Paracoccus pantotrophus* (*Pp*) [9], *Haloarcula marismortui* [10], and *Marinobacter hydrocarbonoclasticus* [11]. The prototypical Nar, *Ec* NarGHI consists of three subunits: NarG bears the Mo active site for nitrate reduction and a [4Fe–4S] cluster, NarH bears three [4Fe–4S] clusters and a [3Fe–4S] cluster, and NarI is attached to the membrane and bears two *b*-type hemes that oxidize quinols [12,13]. The iron–sulfur clusters form a chain of electron-transfer relays from the quinol oxidation site to the Mo; they are numbered from 0 to 4 according to their distance from the Mo active site. Most of the Nars studied so far could be purified as a NarGHI trimer using detergents to stabilize the membrane-bound part, or as a soluble NarGH dimer. Removing the membrane subunit (NarI) completely abolishes the quinol oxidation activity, but has only a moderate effect on the nitrate reductase activity [14].

EPR spectroscopy has been extensively used to obtain structural information about the NarGHI metal centers in their paramagnetic

* Corresponding author.
E-mail address: vincent.fourmond@imm.cnrs.fr (V. Fourmond).

http://dx.doi.org/10.1016/j.bbabio.2015.06.007
0005-2728/

state. The $S = 1/2$ Mo(V) ion at the NarG active site displays two major pH-dependent EPR signatures named from their pH domain of predominance, the so-called "high-pH" and "low-pH" signals [44]. On the basis of the closeness between the pKa value of 8.3 characterizing the pH-dependent equilibrium between these two Mo(V) EPR species and the one controlling the pH-dependence of enzyme activity, Vincent and Bray suggested that only the low-pH Mo(V) form is catalytically active [15]. However this pKa value was determined in the presence of chloride and it was subsequently shown that anion binding modifies the high-pH/low-pH signal transition pKa [16,17]. Later, a pH dependence study of Mo(V) species reduction potentials performed in absence of contaminating anions has suggested that both species could be involved in the catalytic cycle [18]. Clearly, understanding the molecular origin of the transition between the high- and low-pH Mo(V) forms and their catalytic relevance still requires further work.

EPR analyses of the NarGH iron–sulfur clusters in combination with redox potentiometry and site-directed mutagenesis allowed a detailed characterization of their redox and magnetic properties. The higher-potential FS4 and FS1 clusters exhibit well-resolved EPR signatures with features around $g \approx 2$. The FS1 EPR signal is composite, with a major (67%) rhombic component with g-values 2.049, 1.947, 1.869 and a minor (33%) quasi axial component with g-values 2.010, 1.885, 1.871. This was interpreted as arising from a mixture of valence delocalisation in the cubane leading to different g-tensors [19]. The individual EPR spectral contributions of the other lower potential NarH clusters FS2 and FS3 are more difficult to resolve due to their spin–spin interactions with reduced FS1 and FS4. Remarkably, the NarG FS0 cluster has an unusual $S = 3/2$ ground state that gives rise to two peaks at $g = 5.60$ and $g = 5.00$ corresponding to the two low-field resonances of the Kramers doublets [20,21]. Detailed spin quantitation experiments of these signatures show that they account for only 40% of the total FS0 centers present in the enzyme implying that 60% of the FS0 centers is present in another undetected spin state, most likely in the $S = 1/2$ state [21]. The molecular origins of these spectral heterogeneities and whether they are related to functional heterogeneities remain unknown.

Functional information on NarGH has also been obtained using protein film voltammetry (PFV), a technique in which the enzyme is immobilized on an electrode and interfacial electron transfer is direct. The current is proportional to the turnover rate [22]. Initial studies revealed a complex dependence of activity on potential that is a signature of all the NarGH enzymes studied so far [9,23–26], and which shares some features with that of other molybdenum enzymes [27–31]. Field and coworkers [25] have shown that some of their preparations of *Pp* NarGH require to be reduced at low potentials to obtain maximum activity, but it is not known whether this also applies to other Nars.

In this work, we use a combination of PFV and EPR spectroscopy to evidence a reductive activation process in *Ec* NarGH, and to study its kinetics and the relation between inactive species and spectral signatures of the metal centers. We show that *Ec* NarGH is purified in a heterogeneous state in which about 20% to 40% are inactive species that activate upon reduction. The activation proceeds in two steps, the first being a non-redox reversible reaction while the second is an irreversible reduction. The presence of the inactive species correlates neither with the high- and low-pH Mo(V) EPR signatures nor with the heterogeneities of the signatures of the FS0 and FS1 clusters. This means that the chemical transformation between the inactive and active species does not involve the first coordination sphere of these cofactors.

2. Results

2.1. Ec NarGH irreversibly activates the first time it is reduced

Ec NarGH readily adsorbs onto pyrolytic graphite edge (PGE) electrodes to form stable electroactive films [24]. We studied such films using cyclic voltammetry, which consists in sweeping the electrode potential back and forth between two values. The resulting current is shown in Fig. 1. The red trace is the first scan recorded on a film, while the green trace is the subsequent scan. For the latter, the currents of the sweep towards low potential and the sweep towards high potential are identical; they are merely offset by the electrode charging current, obtained in the absence of enzyme (blue trace); this means that during the second scan, the current response is in a steady state. On the first scan however this is not the case, as at each potential, the current of the sweep towards high potential is larger in magnitude than that of the sweep towards low potential; for instance, at −0.2 V (vs SHE) the current on the sweep towards low potential is ≈2.5 μA, while on the sweep towards high potential it is ≈5 μA (black arrow in Fig. 1). This indicates that the activity on the sweep towards high potential is larger than on that towards low potential, which means that the quantity of active enzyme has increased about two-fold during the sweep at low-potentials. The absence of hysteresis on second scan shows that the enzyme has fully activated and that no inactive species have been regenerated upon oxidation. This is confirmed by the fact that subsequent scans are identical to the second one (data not shown).

We tried regenerating the inactive species after activation by oxidizing the enzyme (300 s at 0.64 V) or exposing it to air for 2 h, or to millimolar concentrations of azide, nitrite, nitrate and sulfite but none of these conditions restored the species that activate upon reduction, which shows that the activation is irreversible under these conditions.

While cyclic voltammetry rapidly gives qualitative information about (in)activation processes, it is not adapted to quantitative analysis of their kinetics. A better technique is chronoamperometry, in which the potential varies in a stepwise fashion and the current is recorded as a function of time. We and others have used this technique successfully to gain mechanistic insights on activation/inactivation processes of a number of other enzymes [6,7,32–38].

2.2. About 30% of the enzyme is initially present in either of two inactive forms that activate upon reduction

We submitted fresh films of NarGH to a sequence of two potential steps (Fig. 2). The first step is at a high enough potential (E_1) that catalysis does not occur, the current is therefore null. The potential of the second step, E_2, is such that the enzyme catalyzes the reduction of nitrate. A significant nitrate reduction current is already visible at the beginning of this step, and its magnitude increases slowly over time as the enzyme activates, until a point where current magnitude decreases again (at $t \approx 100$ s in Fig. 2C) because of film loss, i.e. the irreversible

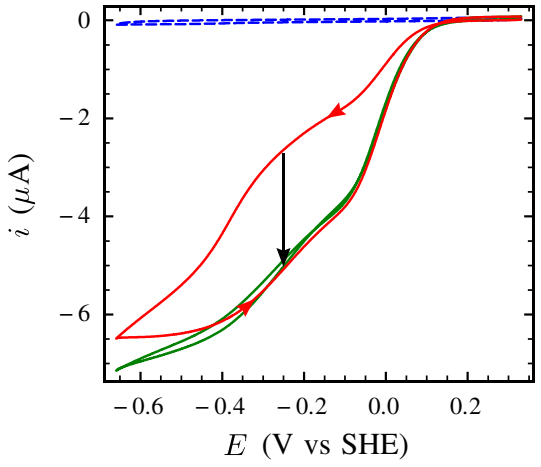

Fig. 1. Cyclic voltammograms of an *Ec* NarGH-coated PGE electrode. The red trace is the first scan recorded on a film, the green trace is the second scan. In blue is a control experiment recorded in the absence of enzyme. Experimental conditions: $T = 40$ °C, pH 5.5, nitrate concentration: 1 mM, scan rate: 10 mV/s, rotation rate: 3.5 krpm.

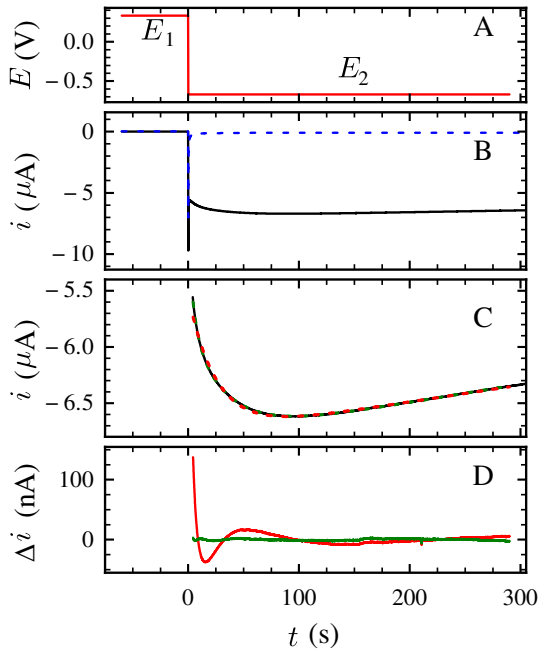

Fig. 2. Chronoamperometry experiment in which an *Ec* NarGH-coated PGE electrode is submitted to a series of potential steps. Panel A: electrode potential as a function of time ($E_1 = 330$ mV and $E_2 = -670$ mV). Panel B: resulting current. The blue dashed line is a control experiment recorded without adsorbed enzyme; it is used as the baseline for the curves shown in panel C. Panel C: baseline-subtracted data (black trace) together with the mono- (red) and bi-exponential fits (green). Panel D: residuals for the mono- (red) and bi- (green) fits. Experimental conditions: $T = 40$ °C, pH 5.5, nitrate concentration 1 mM, electrode rotation rate: 3.5 krpm. Parameters for the mono-exponential fit: $\tau_1 = 26$ s, $\alpha_1 = 0.18$, $k_{loss} = 2.310^{-4}$ s^{-1} and the bi-exponential fit: $\tau_1 = 4.8$ s, $\alpha_1 = 0.11$, $\tau_2 = 33$ s, $\alpha_2 = 0.16$, $k_{loss} = 2.610^{-4}$ s^{-1}.

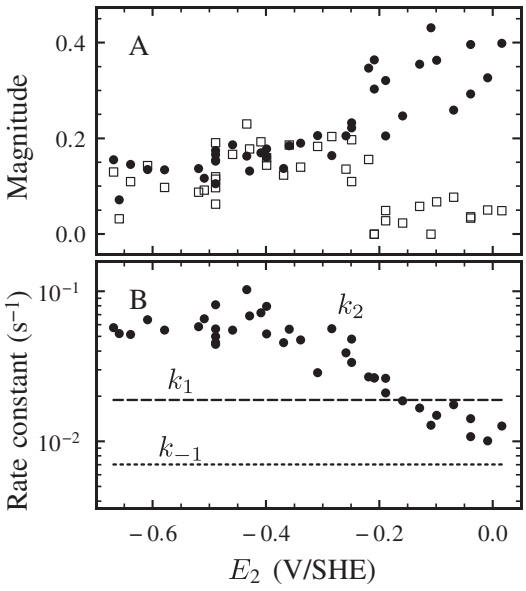

Fig. 3. Results of fits to chronoamperograms such as that in Fig. 2 using different models. Each data point is the result of one fit, and the abscissa is the electrode potential applied to trigger activation. Panel A: amplitudes of the fast (open squares) or slow (filled circles) phases of the bi-exponential fit (the time constants are shown in SI Fig. S1). Panel B: dependence of the best value of the parameter k_2 in model (3) as a function of E_2 (circles), together with the unique values of k_1 and k_{-1} indicated respectively as dashed and dotted horizontal lines (by hypothesis, these two rate constants do not depend on E_2).

desorption of the enzyme [39]. We fitted mono- and biphasic exponential functions (Eq. (1) below) to the traces shown in panel C, which are obtained from those of panel B by subtracting the baseline (the current recorded in the absence of enzyme, shown as a dashed blue line in panel B):

$$i(t) = i_\infty[1-\alpha_1\exp(-t/\tau_1)-\alpha_2\exp(-t/\tau_2)] \times \exp(-k_{loss}t). \quad (1)$$

In this equation, i_∞ is the current that would be obtained asymptotically if there were no film loss, k_{loss} is a first-order rate constant describing film loss [39], α_1 (resp α_2) is the magnitude of the first (resp. second) exponential phase relative to i_∞, and τ_1 (resp. τ_2) its time constant. The origin of time is the beginning of the step at E_2. In the case of a monophasic evolution, $\alpha_2 = 0$ (and τ_2 is not relevant). The sum $\alpha_1 + \alpha_2$ is the fraction of enzyme that activates during the step at E_2, relative to the final amount of active enzyme.

The fits of Eq (1) to the data are plotted in Fig. 2C as red (monophasic, $\alpha_2 = 0$) and green (biphasic, α_2 is a free parameter) traces. The difference between the data and the fits is plotted in the same colors in panel D. The monophasic fit significantly deviates from the data, whereas the difference between the bi-phasic fit and the data is small (just above noise) and evenly distributed around zero, showing that the bi-phasic fit adequately reproduces the data.

To check that this behavior is independent of the activation potential, we repeated this experiment using freshly made films, for a number of values of the potential of the second step (E_2), subtracting a blank recorded under the same conditions, and fitting both a mono- and bi-exponential function (Eq. (1)) to the resulting current trace. We observed that the residuals (sum of squares of the difference of the data minus the fit) of the bi-exponential fits were in average 3.5 times lower than those of the mono-exponential fit. This means that the bi-exponential fit is always significantly better than the mono-exponential one. The amplitudes of the two exponential phases are plotted in Fig. 3A. They correspond to a total of 30 to 40% of initially inactive enzymes in the sample. The fact that both phases have significant amplitudes (at least in the low-potential range) suggests that there are two distinct inactive species. This is confirmed below by the consistency of the results we deduce from this hypothesis.

2.3. The two inactive species interconvert

Different models give rise to a biphasic evolution of the current over time (Eq. (1)) for a given value of E_2, but they cannot be distinguished on the basis of one experiment alone. However, these models give different predictions with respect to how the fit parameters (time constants and amplitudes) depend on the activation potential E_2, and we use these predictions to discriminate between different hypotheses.

In the simplest kinetic model that gives rise to a biphasic irreversible activation (see SI section S1.1), each of the two inactive species, I1 or I2, reacts independently to form the active species A, in an irreversible, first order step:

$$I_1 \xrightarrow{k_{a1}} A \xleftarrow{k_{a2}} I_2. \quad (2)$$

According to this model, the initial fractions of inactive species, that we name I_{10} and I_{20}, are equal to (and can be determined from) the magnitudes of the slow and fast phases relative to the asymptotic current i_∞, i.e. $\alpha_1 = I_{10}$ and $\alpha_2 = I_{20}$ (see SI Eq. S4). Therefore, if this model were correct, the relative magnitudes of the slow and fast phases would be independent of the value of E_2, since the initial fractions of inactive species do not depend on the conditions used for activating the sample. As can be seen in Fig. 3A, the magnitudes of the two phases strongly depend on potential, since they have close values at low potential (about 15–20% for each phase), but at high potentials, the magnitude of the slow phase is much larger than that of the fast phase (30–40% vs 5%). The predictions of model (2) do not match experimental data, therefore, the two inactive species cannot activate independently of each other.

In the following, we thus consider another model, which is the simplest in which the species do not activate independently. According

to this model, the activation proceeds in two sequential steps: the reversible transformation between the two inactive species (forward rate constant k_1 and backward rate constant k_{-1}), followed by an irreversible activation step (rate constant k_2).

$$I_1 \underset{k_{-1}}{\overset{k_1}{\rightleftharpoons}} I_2 \xrightarrow{k_2} A. \quad (3)$$

In this model, the amplitudes of the exponential phases, α_1 and α_2 are complex functions of I_{10}, I_{20} and of the rate constants (see SI Eq. S13). However the total initial proportion of inactive species is still the sum of the amplitudes of the slow and fast phases, like in model (2):

$$\alpha_1 + \alpha_2 = I_{10} + I_{20}. \quad (4)$$

2.4. The transformation between I_1 and I_2 is not redox

To learn about the redox and/or acid/base reactions that occur during the activation, it is useful to interpret how the rate constants k_1, k_{-1} and k_2 depend on the activation potential and on pH. However, determining the three rate constants is not possible without making further assumptions. Indeed, fitting the model (3) to kinetic traces requires adjusting 7 parameters per chronoamperogram: the rate constants k_1, k_{-1} and k_2, the initial concentrations of I1 and I2 (I_{10} and I_{20}), the current of the fully activated film i_a and a rate constant that accounts for film loss, k_{loss}. However, the corresponding equation can be written in the same form as Eq. (1) (see SI Section S1.2), which depends on only 6 parameters (i_∞, k_{loss}, τ_1, τ_2, α_1 and α_2). Thus model (3) is intrinsically underdetermined.

We could lift this indetermination by assuming that the reversible transformation between I1 and I2 is not a redox reaction; this constrains the parameters as follows: (i) k_1 and k_{-1} are independent of the electrode potential E_2, and (ii) as this reaction proceeds even before the making of the film, it is at equilibrium by the time the activation starts, so that $I_{20} = k_1/k_{-1} \times I_{10}$.

Taking these constraints into account, we simultaneously fitted the model to all the activation traces obtained for different values of E_2 (which were already analyzed using Eq. (1) in Fig. 3A), adjusting a single pair of values of k_1 and k_{-1}. Proceeding this way significantly reduces the number of parameters in the fitting procedure. Indeed, fitting a bi-exponential function to n activation traces requires the adjustment of $6 \times n$ parameters (6 per trace); the unconstrained fit of model (3) requires the adjustment of $7 \times n$ parameters (hence the indetermination problem). In contrast, the fit constrained as described above requires the adjustment of only $4 \times n + 2$ parameters: 4 parameters per trace (i_a, k_2, I_{10} and k_{loss}), and 2 parameters that are the same for all traces (k_1 and k_{-1}). This number of parameters is just a little above that of the mono-exponential fit, which requires the adjustment of $4 \times n$ parameters. We found that the residuals of the constrained fits are much closer to the residuals of the unconstrained bi-exponential fits (only 20% higher on average) than to the residuals of the mono-exponential fits, which are 3.5 times greater than the residuals of the bi-exponential fit (data not shown). This is so despite the fact that the overall number of parameters of the constrained fit ($4 \times n + 2 = 162$ for $n = 40$) is much closer to the number of parameters of the mono-exponential fit (160) than the bi-exponential fit (240). Thus, model (3) with the assumption that the first step is not a redox reaction is consistent with the data.

An outcome of this analysis is the dependence of k_2 on electrode potential, which is shown as black dots in Fig. 3B, together with the values of (k_1 and k_{-1} displayed as dashed and dotted horizontal lines. The value of k_2 is constant over a large range of potential at low potential, and decreases when the potential increases, consistent with the fact that the activation slows down at high potential. This is reminiscent of the dependence on potential of the rate of irreversible activation of the high-*g* resting Mo(V) species of *Rs* NapAB [6]. The decrease is very gradual, less steep than a 1-electron sigmoid. The values of k_1 and k_{-1} indicate an initial ratio $I_{20}/I_{10} \approx 3$.

2.5. The transformation between I_1 and I_2 does not involve proton transfer in acidic conditions

We repeated the series of chronoamperometric experiments changing the pH between 5 and 6 (at pH values below 5, the enzyme film is unstable, and at pH values above 6, a very slow reorientation on the electrode occurs that prevents quantitative analysis of the data (data not shown)), and we analyzed the data using the kinetic Scheme (3) as described above (SI Fig. S2). The values of k_1 and k_{-1} do not vary much with pH, and their ratio k_1/k_{-1} does not depend on pH, which means that the interconversion between I1 and I2 is not coupled to the transfer of a proton, at least for pH values below 6. We cannot exclude the possibility of a protonation/deprotonation of pKa greater than 6.

2.6. The inactive species are not related to the low-pH and high-pH Mo(V) spectral signatures

To assess the relationship between the fraction of inactive species detected by electrochemistry and the EPR signatures of the pH-dependent Mo(V) species of the enzyme active site, NarGH samples were prepared at pH 5.5 and 10 and studied by electrochemistry and EPR spectroscopy. Previous spectroscopic studies of samples of *Ec* NarGH and NarGHI have reported two characteristic pH-dependent Mo(V) EPR signals, the so-called "low-pH" and "high-pH" signals, both showing hyperfine coupling with a solvent-exchangeable proton. This coupling is stronger for the low-pH signal which is sensitive to the presence of anions like nitrate, nitrite, chloride and fluoride [16]. The large hyperfine coupling between the unpaired electron of the Mo(V) ion and the $I = 5/2$ nuclear spin of the ^{95,97}Mo isotopes present in ≈25% natural abundance leads to the presence of additional EPR lines that overlap with the major Mo(V) signals arising from the diamagnetic isotopes. This complicates the detailed analysis of Mo(V) EPR spectra especially when several Mo(V) species with partially overlapping signals contribute. Therefore, we have used NarGH preparations enriched in the ^{98}Mo isotope ($I = 0$) throughout this work. The 50 K spectrum of as prepared NarGH at pH 5.5 contains mainly typical low-pH resonances (Fig. 4a, black trace). These constitute a rhombic signal with $g_{av} \approx 1.983$ and a resolved hyperfine splitting of approximately 1 mT due to a single solvent exchangeable proton [40]. In the sample prepared at pH 10, the Mo(V) spectrum has a typical "high-pH" form [8,15] (Fig. 4b, black trace). This signal with $g_{av} \approx 1.976$ has no resolved hyperfine features. Careful examination of the spectra revealed no detectable contribution of the ^{95,97}Mo isotopes, indicating that enrichment of the enzyme with the ^{98}Mo isotope is at least 90%. Interestingly, this approach allowed us to resolve a significant contribution of the low-pH Mo(V) form on the low-field edge of the high-pH Mo(V) signal measured on the pH = 10 sample. This contribution is pointed out by lines in the zoom above trace b in Fig. 4. Spectral simulations (red dotted lines in Fig. 4b) indicate that it accounts for approximately 14% of the total Mo(V) content. Similarly, a significantly better agreement between the simulated (red dotted lines in Fig. 4a) and the experimental Mo(V) spectra of the pH 5.5 sample is found when a weak but significant contribution (approx. 5% of the total Mo(V) signal, green dotted lines in Fig. 4a) of the high-pH Mo(V) form is added to the simulation. The parameters used for spectral simulations shown in Fig. 4 are reported in Table 1.

Table 2 shows the concentrations of the Mo(V) ion in these samples relative to that of the $[3Fe–4S]^{1+}$ cluster (FS4) evaluated from spin quantitation measurements, together with the amount of initially inactive species measured by PFV using the same conditions as in Fig. 2 (all PFV measurements were conducted at pH 5.5, regardless of the pH of the sample). Comparison of the amount of initially inactive

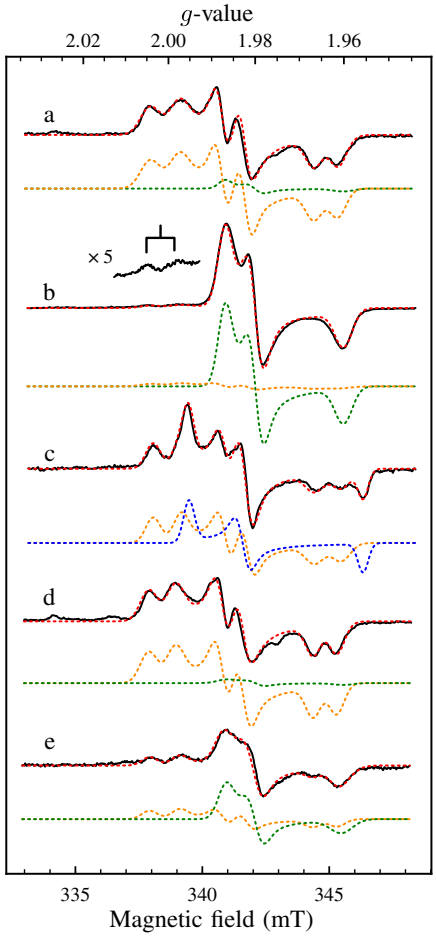

Fig. 4. Experimental (continuous lines) and simulated (red dotted lines) Mo(V) EPR spectra of ^{98}Mo-enriched NarGH. Samples were prepared at pH 5.5 (a, c, d) or pH 10 (b, e). For (c), NarGH has been activated by chemical reduction followed by reoxidation (see text). Spectra (d) and (e) were measured after incubating during 56 h at 4 °C the samples prepared at pH 5.5 and pH 10, respectively. Dotted line spectra under each experimental spectrum correspond to the low-pH (orange), the high-pH (green) or the low g_3 (blue) Mo(V) species. They have been summed up in the following proportions to lead to the red dotted line spectra: (a) 95% low-pH Mo(V) + 5% high-pH Mo(V), (b) 14% low-pH Mo(V) + 86% high-pH Mo(V), (c) 64% low-pH Mo(V) + 36% low g3 Mo(V), (d) % 97 low-pH Mo(V) + 3% high-pH Mo(V), and (e) 48% low-pH Mo(V) + 52% high-pH Mo(V). The trace above spectrum b is a ×5 zoom on the spectral region where the characteristic peaks of the low-pH Mo(V) signature are visible. Measurement conditions: $T = 50$ K, microwave frequency, 9.4806 GHz (a), 9.4771 GHz (b) and 9.4769 GHz (c), 9.48159 GHz (d), 9.48159 GHz (e); microwave power, 0.25 mW; modulation amplitude, 0.2 mT; modulation frequency, 100 kHz. Magnetic fields have been corrected against an offset using a weak pitch sample.

species with those of Mo(V) species reveals that in the pH 5.5 sample (indicated as "$t = 0$" in table 2), there is about twice as much low-pH Mo(V) species as initially inactive species. Similarly, in the pH 10 "$t = 0$" sample, there is twice as much high-pH Mo(V) species as initially inactive species. This suggests that neither the low-pH nor the high-pH form of the Mo(V) ion correlates with the initially inactive species that activate upon reduction.

To further examine the correlation (or lack thereof) between the inactive species and the Mo(V) signatures, we took advantage of the fact that the amount of activable enzyme slowly evolves over time when the sample is kept at 4 °C (SI Fig. S3). We let the pH 5.5 and pH 10 samples described above evolve under anaerobic conditions at 4 °C inside the glove box for several days. While sample aging induces only minor changes of the Mo(V) EPR signal in the sample prepared at pH 5.5 (trace d in Fig. 4), a two-fold increase of the amount of inactive species is measured by chronoamperometry in this sample (Table 2). In contrast, the proportion of initially inactive enzyme of the pH 10 sample (≈20%) does not evolve over time whereas the concentrations of Mo(V) species evolve significantly between the $t = 0$ and $t = 56$ h samples, with a three-fold decrease of the concentration of the high-pH Mo(V) and a two-fold increase of that of the low-pH Mo(V) species (the spectra at $t = 56$ h are shown as traces d and e in Fig. 4). This further confirms that initially inactive species are unrelated to the Mo(V) low-pH and high-pH EPR signals.

2.7. The inactive species are not related to the composite EPR signatures of FS0 and FS1

Having ruled out that the inactive species are linked to either of the major Mo(V) signatures, we wondered if the initial functional heterogeneity (presence of inactive and active species) is related to the spectral heterogeneities displayed by the FS0 [21] and FS1 clusters [19]. We therefore subjected the previously studied pH 5.5 preparation of ^{98}Mo-enriched NarGH to a reversible redox titration as follows. From the initial state, whose redox potential was measured at ≈+240 mV (the corresponding Mo(V) signals are shown in Fig. 4a), we first reduced the sample with sodium dithionite to −101 mV to observe the signatures of both FeS clusters, and then to −300 mV, leaving the sample to evolve long enough (i.e. ≈30 min) at this potential to fully activate. We then reoxidized the sample with potassium ferricyanide to −92 mV to evaluate the effect of the activation on the signature of the FeS clusters, and then back to +240 mV to examine the Mo(V) signal. At each of these steps, we collected two aliquots of the sample: one that was analyzed by EPR spectroscopy, and another one to determine the amount of inactive species using PFV (using the same conditions as in Fig. 2). In the first three samples (+240, −101 and −300 mV), we detected 30% of activable species, while in the next two (−92 and +240 mV), there is essentially none left. That the −300 mV sample still significantly activates is consistent with the sample being examined in PFV at the beginning of the −300 mV poise, before the activation is complete.

Spin quantitation of the Mo(V) EPR signals indicates that the total concentration of the Mo(V) species relative to that of the $[3Fe\text{–}4S]^{1+}$ remains unchanged in the samples poised at +240 mV before and after enzyme activation (data not shown). After activation, the Mo(V) EPR spectrum consists of a mixture of low-pH Mo(V) species and of an additional Mo(V) species (Fig. 4c). The latter has a rhombic signature with $g_1 = 1.996$, $g_2 = 1.984$ and $g_3 = 1.956$ and is hereafter referred to as "low g_3" Mo(V) species. The spectral simulations shown in Fig. 4c indicate that it accounts for ≈36% of the total Mo(V) content. This species has been previously observed after reduction of nitrate reductase with sodium dithionite and reoxidation with nitrate [40,15] and it was suggested to arise from a non-functional species. That this species is not detected as "initially inactive species" in PFV experiments after activation suggests that it does not activate upon reduction.

Table 1
EPR parameters used to simulate the Mo(V) signals recorded in ^{98}Mo-enriched NarGH prepared at pH 5.5 and pH 10 and shown in Fig. 4. We estimate that the *g*-values are accurate to 0.0005 and the A-values to 0.1 mT.

Mo(V) species	g_1	g_2	g_3	g_{av}	Anisotropy g_1–g_3	Rhombicity $(g_1–g_2)$ / $(g_1–g_3)$	A_1 (mT)	A_2 (mT)	A_3 (mT)
Low-pH	2.0009	1.9847	1.9638	1.9831	0.0371	0.4366	1.2	0.9	0.9
High-pH	1.9869	1.9800	1.9601	1.9757	0.0268	0.2575			
Low g_3	1.9952	1.9828	1.9557	1.9780	0.0395	0.3139			

Table 2
Relative proportion of the low-pH, high-pH and low g_3 Mo(V) species (expressed in spin/molecule) in various preparations, estimated with respect to the amount of FS4 as described in Materials & methods section and assuming one FS4 per enzyme. The last row gives the concentration of initially inactive species determined by PFV experiments using the same conditions as those of Fig. 2 (systematically at pH 5.5), expressed as a fraction of the final activity. nd: Not detected.

Mo(V) species/FS4	pH 5.5, $t = 0$ (4a)	pH 5.5, $t = 56$ h (4d)	pH 10, $t = 0$ (4b)	pH 10, $t = 56$ h (4e)	pH 5.5, after activation (4c)
Low-pH Mo(V)	0.41 ± 0.03	0.44 ± 0.04	0.07 ± 0.02	0.13 ± 0.02	0.19 ± 0.02
High-pH Mo(V)	0.020 ± 0.015	0.013 ± 0.010	0.41 ± 0.04	0.14 ± 0.02	nd
Low g_3 Mo(V)	nd	nd	nd	nd	0.10 ± 0.02
$I_{10} + I_{20}$	0.23 ± 0.03	0.45 ± 0.03	0.20 ± 0.05	0.20 ± 0.05	0.02 ± 0.01

EPR spectra of the $S = 3/2$ FS0 $[4Fe–4S]^{1+}$ cluster before and after activation are shown in Fig. 5a and b, respectively. No variation of the shape or of the amplitude of the two low-field components at $g = 5.0$ and $g = 5.6$ of the rhombic signatures associated to the two Kramers doublets is observed.

The composite EPR signal of the $[4Fe–4S]^{1+}$ FS1 cluster before and after activation is shown in Fig. 5c and d, respectively. Both spectra could be satisfactorily simulated (dotted lines in Fig. 5c–d) by superimposing a major (67%) rhombic component with $g_1 = 2.049$, $g_2 = 1.946$ and $g_3 = 1.868$ and a minor (33%) quasi-axial component (with $g_1 = 2.011$, $g_2 = 1.882$ and $g_3 = 1.871$) in agreement with previously published data [19]. This shows that the activation process has no significant effect on the FS1 composite signal either.

Overall, our results show that there is no correlation between initially inactive species and the spectral heterogeneity of FS0 and FS1.

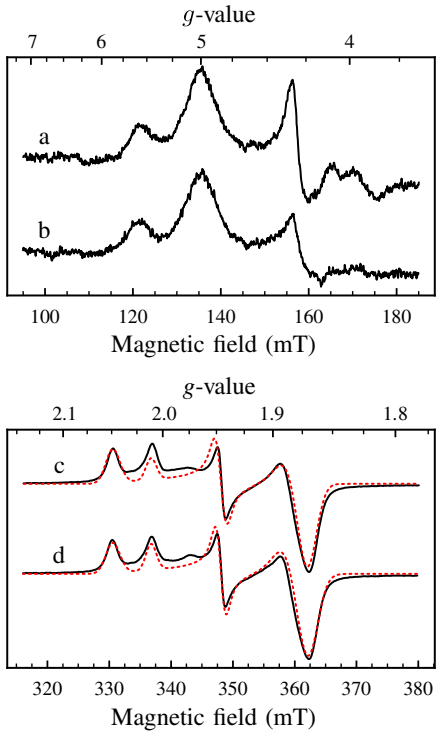

Fig. 5. EPR spectra of FS0 (a, b) and FS1 (c, d) before (a, c) and after (b, d) a 30 min-long poise at −300 mV. The isotropic signal at $g = 4.3$ (a, b) is due to the presence of adventitious Fe^{3+} ions. The red dashed lines in c) and d) are spectral simulations obtained by superimposing a major (67%) rhombic component with $(g_1, g_2, g_3) = (2.049, 1.946, 1.869)$ and a minor (33%) quasi-axial component with $(g_1, g_2, g_3) = (2.011, 1.882, 1.871)$ using g-strain parameters $(\sigma_1, \sigma_2, \sigma_3) = (0.007, 0.004, 0.007)$ for the rhombic component, and $(\sigma_1, \sigma_2, \sigma_3) = (0.005, 0.009, 0.008)$ for the quasi-axial component. Experimental conditions: $T = 12.5$ K, microwave frequency, 9.4769 GHz (a, c), 9.4817 GHz (b, d); microwave power, 103 mW; modulation amplitude, 1 mT (a, b), 0.5 mT (c, d); modulation frequency, 100 kHz. Samples are poised at −101 mV (a, c) or −92 mV (b, d).

3. Discussion

Several members of the Mo/W-*bis*PGD enzyme family were purified in a mixture of species, some of which become active upon reduction. This was first described in the case of the soluble DMSO reductase, through the observation that a cycle of reduction and reoxidation increases both the homogeneity of the UV/Visible molybdenum signatures and the DMS oxidation activity [5,41–43]. The inactive species was assigned to a form of the enzyme in which the two thiolate ligands of a pterin have reversibly dissociated from the Mo. Some of us observed a similar reductive activation with another member of the Mo/W-*bis*PGD family, *Rs* periplasmic nitrate reductase NapAB. We have shown that the inactive species gives the so-called Mo(V) high-*g* resting signal [6], and proposed that the inactivation is due to one of the pterin being in an oxidized open conformation [7]. Using PFV, Field and coworkers have also observed such a reductive activation with samples of *Pp* Nar [25], an enzyme closely related to *Ec* Nar, the subject of this paper. They showed that *Pp* Nar activates the first time it is reduced, independently of the presence of nitrate.

In this work, we have shown that *Ec* Nar also activates the first time it is reduced, and that the initially inactive species that are activated upon reduction amount to 20 to 40% of the final quantity of active enzyme. The fact that a dithionite-reduced sample (such as that giving spectrum b in Fig. 5) does not show reductive activation indicates that this activation is not an artifact of the interaction of the enzyme with the electrode. The activation process appears irreversible, in that we could not regenerate the initially inactive state after the enzyme had been activated, which is also what we found in the case of *Rs* NapAB [6]. We studied the kinetics of activation using protein film voltammetry. With an original approach in which we fitted all the kinetic traces at a given pH at once to constrain the fit parameters, we were able to show that (i) the inactive species exists under two different forms, and that (ii) the activation proceeds sequentially, first through a reversible reaction involving neither proton (at least at pH values below 6) nor electron transfer, and second through an irreversible reduction giving the active form.

We observed that in samples equilibrated at pH 5.5 and left to evolve at 4 °C, the amount of activable species slowly increased over time from 20% in as-purified enzymes to about 40% after a week (after which the fraction of inactive form no longer evolves). The chemical changes underlying this slow transformation are unknown. This increase in the concentration of activable species could result from inactivation of previously active species, which would suggest that the activation is in fact reversible but that the inactivation is very slow. Alternatively, it could result from the transformation of another inactive species that does not activate upon reduction.

The presence of a significant amount of inactive species in the as-prepared samples (those that were used for spectroscopic investigations) raises the question of whether some of the spectroscopic signatures recorded on Nar are that of the inactive species, as it occurs in *Rs* NapAB. To address this issue, we investigated the relation of the inactivation with the major Mo(V) EPR signatures, the so-called low-pH and high-pH Mo(V) signatures. We concluded that they are not related to the inactive species that activate upon reduction because: (i) there are conditions

under which either one Mo(V) signal or the other amounts to a fraction of enzyme that is significantly larger than the fraction that activates, and (ii) the evolution over time of the proportion of inactive enzyme and of the Mo(V) species are anti-correlated: at pH 5.5, the inactive fraction evolves while the fraction of Mo(V) species does not and at pH 10, the opposite is observed. This shows that neither of these Mo(V) signatures arises from the inactive species that activate upon reduction. Overall, these results are consistent with the previous proposal by some of us that the high-pH and the low-pH forms of the Mo(V) are both involved during the redox turnover of the enzyme [18]. It should be emphasized however that, from our data, we cannot rule out the possibility that these forms correspond to inactive species that do not activate under the conditions we used.

Upon discovery, the species giving the high-pH and low-pH signatures were proposed to be respectively the basic and acidic forms of a unique protonable species. This was supported by the fact that a solvent-exchangeable proton was detected in the low-pH signal, but not in the high-pH one, and this proton was thought to be the acidic proton [15]. This hypothesis was weakened upon the discovery of a solvent-exchangeable proton coupled to the Mo(V) in the high-pH form, although the coupling is weaker [16]. Thanks to the use of preparations enriched in ^{98}Mo, we could detect small proportions of the high-pH form at pH 5.5 and of the low-pH form at pH 10, and quantify them. In the light of our data, the proposition that the low- and high-pH forms are in an acid/base equilibrium becomes unlikely, for two reasons (i) during the course of the exposure of the pH 10-equilibrated sample at 4 °C, the ratio of the low-pH over high-pH form evolves from 17% to 93%, which is not consistent with the fact that, as the pH remains constant in the buffered solution, the ratio should not change; and (ii) if the low-pH and high-pH forms were in acid-base equilibrium, the mass action law implies that their ratio would be proportional to the concentration of protons. However, the ratio of low-pH/high-pH forms changes from ≈30 at pH 5.5 to ≈0.2 at pH 10 (or ≈1 if one considers the data at $t = 56$ h), which gives at best a change of 200 over 4.5 pH units. This is two orders of magnitude below the $10^{4.5}$ expected if it were a true acid/base equilibrium.

The FS0 and FS1 iron–sulfur clusters of NarGH show composite EPR signatures in as-prepared samples. To assess whether this heterogeneity is related to the inactive species, we performed a reversible redox titration, in which spectra are recorded twice at a given potential, once before and once after a low potential poise that activates the enzyme. This had no detectable effect on the signatures of the FS0 and FS1 clusters, which suggests that the activation process is not related to the FS0 and FS1 clusters.

Our redox cycling experiment performed at pH 5.5 reveals the appearance of the low g_3 Mo(V) species which then overlaps with the major low-pH species and accounts for about 40% of the total Mo(V) content. Comparison of the principal values of its g-tensor with those measured for Mo(V) species in mononuclear molybdoenzymes suggests that the low g_3 species arises from a molybdenum cofactor in which one pterin ligand has dissociated from the Mo ion. A similar conclusion has been drawn for the low g signal detected in periplasmic nitrate reductases [4]. This structural interpretation of EPR spectroscopic data is consistent with the previous assignment by Bray and coworkers of the low g_3 Mo(V) signal to a non-functional species [15,40].

In summary, we have characterized the kinetics of reductive activation of *Ec* NarGH, and we have shown that it has no observable effect on the major Mo(V) signatures and of the FS0 and FS1 clusters. This means that the chemical change that transforms the inactive species into the active one is sufficiently remote from these centers that it does not affect their spin-carrying orbitals. The fact that the activation proceeds via a reduction implies that the change must nonetheless occur close enough to one of the redox-active centers of NarGH. One possibility is that, as proposed for *Rs* NapAB, the activation is linked to a chemical change in one of the pterins [7], which may be related to the fact that two crystal structures were obtained of *Ec* Nar that differ, in particular, by the fact that the Q pterin (the one distal from FS0) has an open [12] or a closed [13] ring. In Nap, we could detect this change via a modification of the coupling between the Mo(V) and the nearby reduced FeS. In Nar, such a coupling could not be detected because the FS0 cluster and the Mo atom are not simultaneously paramagnetic due to their redox properties. Alternatively, it is possible that the activation is linked to a change in conformation in one of the low-potential iron–sulfur clusters. Unfortunately their individual EPR signatures are not observable due to large intercenter magnetic couplings, which makes it very difficult to follow chemical changes in their vicinity.

The origin of the inactive species remains to be determined. It is possible that they are the result of slow oxidative damage, or it may be as well that the reduction that activates the enzyme is the final step in the maturation of the enzyme. Under normal physiological conditions, the nitrate reductase complex is reduced by the quinone pool via the NarI quinol oxidase domain. One may consider that the activation step thus occurs in vivo as long as the NarGH complex is connected to NarI, a situation not encountered in our study with the purified soluble NarGH dimer. This mechanism may actually be general in the Mo/W-*bis*PGD enzyme family, which is supported by the fact that such a reductive activation has been observed on two other members of this family, and often on recombinant overexpressed enzymes, for which either the natural redox partner is absent [41,43] or not overexpressed [6,7], so that the final reduction step never occurs.

4. Material and methods

4.1. Purification of Ec NarGH

Ec cells transformed with plasmid pNarGH$_{His6}$J were grown under aerobic conditions in minimal medium supplemented with $^{98}MoO_4^{2-}$, 2 μM (ORNL, Tenessee, USA).

We purified the protein in one step by affinity chromatography, as described earlier [21]. Buffered solutions at pH 5.5 and 10.0 were 50 mM MES and CAPS, respectively. All solutions contained EDTA (1 mM).

All the samples were stored inside a glovebox filled with N_2 ($p_{O_2} < 5$ ppm) at 4 °C (for the samples used in electrochemical experiments and time evolution of EPR spectra) or −80 °C (for the sample used in redox titration).

4.2. Titration experiments and EPR spectroscopy

4.2.1. Samples

All as-prepared EPR samples and those after 56 h at 4 °C were prepared in the glovebox and frozen by quenching the EPR tube in a cold ethanol solution (≈200 K). The redox titration was performed in an anaerobic cell flushed with argon. A cocktail of mediators (10 μM each of 2,6-dichloroindiphenol, 2,5-dimethyl-p-benzoquinone, 1,2-naphtoquinone, phenazine methosulfate, phenazine ethosulfate, methylene blue, resorufin, indigo carmine, anthraquinone 2,6-disulfate and phenosafranine) was added to accelerate the redox equilibration. Reduction and oxidation steps were performed by injecting small volumes (2 to 5 μL) of solutions of 50 mM Na-dithionite and 10 mM $K_3Fe(CN)_6$, respectively. Samples were anaerobically frozen in liquid nitrogen (77 K) after equilibration.

4.2.2. EPR spectroscopy and spectral simulations

X-band EPR spectra were recorded using a Bruker-Biospin EleXsys E500 spectrometer equipped with a standard rectangular Bruker EPR cavity fitted to an Oxford Instruments helium flow cryostat. Mo(V) signatures were recorded using experimental conditions that avoid overmodulation or saturation and allow proper parameterization for the simulation of g-tensors, lineshapes and proton hyperfine coupling.

Simulations of frozen solution EPR spectra were carried out using the EasySpin [44] package (release 4.5.5) that works under MatLab (The MathWorks, Inc., Natick). Experimental magnetic fields were corrected for an offset against a standard with known g-value (weak pitch, $g = 2.0028$). Experimental Mo(V) spectra were then simulated by adding the contribution of two independent species (as described in the legend of Fig. 4). Anisotropic spectral broadening was taken into account through unresolved hyperfine couplings (HStrain function) or uncorrelated g strain effects (gStrain function) for simulations of Mo(V) or FS1 EPR spectra, respectively. The Hstrain parameters correspond to the full width at half maximum (in MHz) of Gaussian lines along the three g-tensor principal axes. These were adjusted to $(22 \pm 4{,}16 \pm 3{,}20 \pm 3)$, $(20 \pm 4{,}18 \pm 2{,}25 \pm 3)$, and $(14 \pm 4{,}16 \pm 2{,}13 \pm 1)$ for the simulations of the low-pH, high-pH and low g_3 Mo(V) species, respectively. For g-strain effects, the full widths at half maximum characterized by standard deviations (σ_1, σ_2, σ_3) of the Gaussian distributions of the principal g-values (g_1, g_2, g_3) are assumed to be completely uncorrelated. Simulations of the low-pH Mo(V) species were carried out by considering an additional proton hyperfine coupling tensor with principal axes assumed to be collinear to those of the Mo(V) g-tensor. Quantitation of the total Mo(V) content in a sample was achieved by comparing the double integral of the Mo(V) EPR signal measured at 50 K with the double integral of the oxidized FS4 signal measured at 12.5 K, 100 mW microwave power and 0.5 mT modulation amplitude at 100 kHz and corrected to account for weak saturation effects of the FS4 signal in these conditions. Each individual Mo(V) species was then quantitated on the basis of their proportion relative to that of the total Mo(V) content as inferred from spectral simulation.

4.3. Electrochemical experiments

The electrochemical setup has been described previously [6]. All electrochemical experiments were carried out in an anaerobic glovebox (JACOMEX) filled with N_2 (residual O2 < 5 ppm). To form the enzyme films, we polished the pyrolitic graphite-edge electrode (surface approx 2 mm^2) with an alumina slurry (Buehler, 1 μm), then we painted it with 0.6–0.8 μL of a solution of NarGH (1–2 μM, pH 5.5 or 10.0). Buffers used in electrochemical experiments contained 5 mM of each of MES, sodium acetate, HEPES, TAPS and CHES and 0.1 M NaCl, pH 5.5 (excepted for the results described in Section 2.5, for which the buffer was the same, but titrated to pH values between 5 and 6). We analyzed and fitted the data using in-house programs called SOAS [45] and QSoas, available on our Website at http://www.qsoas.org. Both programs embed the ODRPACK software for non-linear least squares regressions [46]. All data were plotted using ctioga2 (http://ctioga2.sourceforge.net). All potentials are quoted with respect to the standard hydrogen electrode.

Transparency document

The Transparency document associated with this article can be found, in the online version.

Acknowledgments

The authors are grateful to Léa Sylvi for her expert assistance in the preparation of NarGH samples, to Dr. Emilien Etienne for the maintenance of the EPR instrumentation, and to Dr. Frédéric Biaso for helpful discussions. This work was funded by the French National Research Agency (ANR, project MC2, http://anrmc2.wordpress.com, grant number 11-BSV5-005-01), the A*Midex foundation of Aix-Marseille University (project MicrobioE, grant number ANR-11-IDEX-0001-02), and the CNRS for the project "Émergence CO2" from the "Mission interdisciplinarité". We acknowledge the national french EPR network (RENARD, IR3443, http://renard.univ-lille1.fr). Julia Rendon was supported by a CNRS/Région Provence Alpes Côte d'Azur PhD fellowship. The authors are part of the French Bioinorganic Chemistry group (http://frenchbic.cnrs.fr).

Appendix A. Supplementary data

Supplementary data to this article can be found online at http://dx.doi.org/10.1016/j.bbabio.2015.06.007.

References

[1] S. Grimaldi, B. Schoepp-Cothenet, P. Ceccaldi, B. Guigliarelli, A. Magalon, The prokaryotic Mo/W-bisPGD enzymes family: a catalytic workhorse in bioenergetic, Biochim. Biophys. Acta 1827 (8–9) (2013) 1048–1085, http://dx.doi.org/10.1016/j.bbabio.2013.01.011.
[2] R.A. Rothery, G.J. Workun, J.H. Weiner, The prokaryotic complex iron–sulfur molybdoenzyme family, Biochim. Biophys. Acta 1778 (2008) 1897–1929, http://dx.doi.org/10.1016/j.bbamem.2007.09.002.
[3] M.J. Pushie, G.N. George, Spectroscopic studies of molybdenum and tungsten enzymes, Coord. Chem. Rev. 255 (2011) 1055–1084, http://dx.doi.org/10.1016/j.ccr.2011.01.056.
[4] F. Biaso, B. Burlat, B. Guigliarelli, DFT investigation of the molybdenum cofactor in periplasmic nitrate reductases: structure of the Mo(V) EPR-active species, Inorg. Chem. 51 (2012) 3409–3419, http://dx.doi.org/10.1021/ic201533p.
[5] R. Bray, B. Adams, A. Smith, B. Bennett, S. Bailey, Reversible dissociation of thiolate ligands from molybdenum in an enzyme of the dimethyl sulfoxide reductase family, Biochemistry 39 (37) (2000) 11258–11269, http://dx.doi.org/10.1021/bi0000521.
[6] V. Fourmond, B. Burlat, S. Dementin, P. Arnoux, M. Sabaty, S. Boiry, B. Guigliarelli, P. Bertrand, D. Pignol, C. Léger, Major Mo(V) EPR signature of *Rhodobacter sphaeroides* periplasmic nitrate reductase arising from a dead-end species that activates upon reduction. Relation to other molybdoenzymes from the DMSO reductase family, J. Phys. Chem. B 112 (48) (2008) 15478–15486, http://dx.doi.org/10.1021/jp807092y.
[7] J.G. Jacques, V. Fourmond, P. Arnoux, M. Sabaty, E. Etienne, S. Grosse, F. Biaso, P. Bertrand, D. Pignol, C. Léger, B. Guigliarelli, B. Burlat, Reductive activation in periplasmic nitrate reductase involves chemical modifications of the Mo-cofactor beyond the first coordination sphere of the metal ion, Biochim. Biophys. Acta 1837 (2) (2014) 277–286, http://dx.doi.org/10.1016/j.bbabio.2013.10.013.
[8] D. Dervartanian, P. Forget, The bacterial nitrate reductase EPR studies on the enzyme a of *Escherichia coli* K12, Biochim. Biophys. Acta (BBA) Protein Struct. 379 (1) (1975) 74–80, http://dx.doi.org/10.1016/0005-2795(75)90009-4.
[9] L.J. Anderson, D.J. Richardson, J.N. Butt, Using direct electrochemistry to probe rate limiting events during nitrate reductase turnover, Faraday Discuss. 116 (116) (2000) 155–169, http://dx.doi.org/10.1039/b000946f.
[10] K. Yoshimatsu, T. Iwasaki, T. Fujiwara, Sequence and electron paramagnetic resonance analyses of nitrate reductase NarGH from a denitrifying halophilic euryarchaeote *Haloarcula marismortui*, FEBS Lett. 516 (1–3) (2002) 145–150, http://dx.doi.org/10.1016/S0014-5793(02)02524-3.
[11] C. Correia, S. Besson, C.D. Brondino, P.J. González, G. Fauque, J. Lampreia, I. Moura, J.J.G. Moura, Biochemical and spectroscopic characterization of the membrane-bound nitrate reductase from *Marinobacter hydrocarbonoclasticus* 617, J. Biol. Inorg. Chem. 13 (8) (2008) 1321–1333, http://dx.doi.org/10.1007/s00775-008-0416-1.
[12] M.G. Bertero, R.A. Rothery, M. Palak, C. Hou, D. Lim, F. Blasco, J.H. Weiner, N.C.J. Strynadka, Insights into the respiratory electron transfer pathway from the structure of nitrate reductase A, Nat. Struct. Mol. Biol. 10 (9) (2003) 681–687, http://dx.doi.org/10.1038/nsb969.
[13] M. Jormakka, D. Richardson, B. Byrne, S. Iwata, Architecture of NarGH reveals a structural classification of mo-bismgd enzymes, Structure 12 (1) (2004) 95–104, http://dx.doi.org/10.1016/j.str.2003.11.020.
[14] B. Guigliarelli, A. Magalon, M. Asso, P. Bertrand, C. Frixon, G. Giordano, F. Blasco, Complete coordination of the four Fe–S centers of the β subunit from *Escherichia coli* nitrate reductase. physiological, biochemical, and EPR characterization of site-directed mutants lacking the highest or lowest potential [4Fe–4S] clusters, Biochemistry 35 (15) (1996) 4828–4836, http://dx.doi.org/10.1021/bi952459p.
[15] S.P. Vincent, R.C. Bray, Electron-paramagnetic-resonance studies on nitrate reductase from *Escherichia coli* K12, Biochem. J. 171 (3) (1978) 639–647 (URL http://www.biochemj.org/bj/171/bj1710639.htm).
[16] G.N. George, R.C. Bray, F.F. Morpeth, D.H. Boxer, Complexes with halide and other anions of the molybdenum centre of nitrate reductase from *Escherichia coli*, Biochem. J. 227 (3) (1985) 925–931 (URL http://www.biochemj.org/bj/227/bj2270925.htm).
[17] G.N. George, N.A. Turner, R.C. Bray, F.F. Morpeth, D.H. Boxer, S.P. Cramer, X-ray-absorption and electron-paramagnetic-resonance spectroscopic studies of the environment of molybdenum in high-pH and low-pH forms of *Escherichia coli* nitrate reductase, Biochem. J. 259 (3) (1989) 693–700 (URL http://www.biochemj.org/bj/259/bj2590693.htm).
[18] A. Magalon, M. Asso, B. Guigliarelli, R. Rothery, P. Bertrand, G. Giordano, F. Blasco, Molybdenum cofactor properties and [Fe–S] cluster coordination in *Escherichia coli* nitrate reductase A: investigation by site-directed mutagenesis of the conserved His-50 residue in the NarG subunit, Biochemistry 37 (20) (1998) 7363–7370, http://dx.doi.org/10.1021/bi972858f.
[19] B. Guigliarelli, M. Asso, C. More, V. Augier, F. Blasco, J. Pommier, G. Giordano, P. Bertrand, EPR and redox characterization of iron–sulfur centers in nitrate reductases

A and Z from *Escherichia coli*, Eur. J. Biochem. 207 (1) (1992) 61–68, http://dx.doi.org/10.1111/j.1432-1033.1992.tb17020.x.
[20] R.A. Rothery, M.G. Bertero, R. Cammack, M. Palak, F. Blasco, N.C.J. Strynadka, J.H. Weiner, The catalytic subunit of *Escherichia coli* nitrate reductase A contains a novel [4Fe–4S] cluster with a high-spin ground state, Biochemistry 43 (2004) 5324–5333, http://dx.doi.org/10.1021/bi049938l.
[21] P. Lanciano, A. Savoyant, S. Grimaldi, A. Magalon, B. Guigliarelli, P. Bertrand, New method for the spin quantitation of $[4Fe–4S]^{+}$ clusters with $S = 3/2$. Application to the FS0 center of the NarGHI nitrate reductase from *Escherichia coli*, J. Phys. Chem. B 111 (48) (2007) 13632–13637, http://dx.doi.org/10.1021/jp075243t.
[22] C. Léger, P. Bertrand, Direct electrochemistry of redox enzymes as a tool for mechanistic studies, Chem. Rev. 108 (7) (2008) 2379–2438, http://dx.doi.org/10.1021/cr0680742.
[23] L. Anderson, D. Richardson, J. Butt, Catalytic protein film voltammetry from a respiratory nitrate reductase provides evidence for complex electrochemical modulation of enzyme activity, Biochemistry 40 (38) (2001) 11294–11307, http://dx.doi.org/10.1021/bi002706b.
[24] S. Elliott, K. Hoke, K. Heffron, M. Palak, R. Rothery, J. Weiner, F. Armstrong, Voltammetric studies of the catalytic mechanism of the respiratory nitrate reductase from *Escherichia coli*: how nitrate reduction and inhibition depend on the oxidation state of the active site, Biochemistry 43 (3) (2004) 799–807, http://dx.doi.org/10.1021/bi035869j.
[25] S.J. Field, N.P. Thornton, L.J. Anderson, A.J. Gates, A. Reilly, B.J.N. Jepson, D.J. Richardson, S.J. George, M.R. Cheesman, J.N. Butt, Reductive activation of nitrate reductases, Dalton Trans. (21) (2005) 3580–3586, http://dx.doi.org/10.1039/b505530j.
[26] J. Marangon, P.M. Paes de Sousa, I. Moura, C.D. Brondino, J.J.G. Moura, P.J. González, Substrate-dependent modulation of the enzymatic catalytic activity: reduction of nitrate, chlorate and perchlorate by respiratory nitrate reductase from *Marinobacter hydrocarbonoclasticus* 617, Biochim. Biophys. Acta 1817 (7) (2012) 1072–1082, http://dx.doi.org/10.1016/j.bbabio.2012.04.011.
[27] P. Bertrand, B. Frangioni, S. Dementin, M. Sabaty, P. Arnoux, B. Guigliarelli, D. Pignol, C. Léger, Effects of slow substrate binding and release in redox enzymes: theory and application to periplasmic nitrate reductase, J. Phys. Chem. B 111 (34) (2007) 10300–10311, http://dx.doi.org/10.1021/jp074340j.
[28] B. Frangioni, P. Arnoux, M. Sabaty, D. Pignol, P. Bertrand, B. Guigliarelli, C. Léger, In *Rhodobacter sphaeroides* respiratory nitrate reductase, the kinetics of substrate binding favors intramolecular electron transfer, J. Am. Chem. Soc. 126 (5) (2004) 1328–1329, http://dx.doi.org/10.1021/ja0384072.
[29] V. Fourmond, B. Burlat, S. Dementin, M. Sabaty, P. Arnoux, E. Étienne, B. Guigliarelli, P. Bertrand, D. Pignol, C. Léger, Dependence of catalytic activity on driving force in solution assays and protein film voltammetry: insights from the comparison of nitrate reductase mutants, Biochemistry 49 (11) (2010) 2424–2432, http://dx.doi.org/10.1021/bi902140e.
[30] K. Heffron, C. Léger, R. Rothery, J. Weiner, F. Armstrong, Determination of an optimal potential window for catalysis by *E. coli* dimethyl sulfoxide reductase and hypothesis on the role of Mo(V) in the reaction pathway, Biochemistry 40 (10) (2001) 3117–3126, http://dx.doi.org/10.1021/bi002452u.
[31] A.J. Gates, D.J. Richardson, J.N. Butt, Voltammetric characterization of the aerobic energy-dissipating nitrate reductase of *Paracoccus pantotrophus*: exploring the activity of a redox-balancing enzyme as a function of electrochemical potential, Biochem. J. 409 (1) (2008) 159–168, http://dx.doi.org/10.1042/BJ20071088.
[32] H. Heering, J. Weiner, F. Armstrong, Direct detection and measurement of electron relays in a multicentered enzyme: voltammetry of electrode-surface films of *E. coli* fumarate reductase, an iron–sulfur flavoprotein, J. Am. Chem. Soc. 119 (48) (1997) 11628–11638, http://dx.doi.org/10.1021/ja9723242.
[33] A. Jones, S. Lamle, H. Pershad, K. Vincent, S. Albracht, F. Armstrong, Enzyme electrokinetics: electrochemical studies of the anaerobic interconversions between active and inactive states of *Allochromatium vinosum* [NiFe]-hydrogenase, J. Am. Chem. Soc. 125 (28) (2003) 8505–8514, http://dx.doi.org/10.1021/ja035296y.
[34] S.E. Lamle, S.P.J. Albracht, F.A. Armstrong, Electrochemical potential step investigations of the aerobic interconversions of [NiFe]-hydrogenase from *Allochromatium vinosum*: insights into the puzzling difference between unready and ready oxidized inactive states, J. Am. Chem. Soc. 126 (45) (2004) 14899–14909, http://dx.doi.org/10.1021/ja047939v.
[35] H. Wijma, L. Jeuken, M. Verbeet, F. Armstrong, G. Canters, Protein film voltammetry of copper-containing nitrite reductase reveals reversible inactivation, J. Am. Chem. Soc. 129 (27) (2007) 8557–8565, http://dx.doi.org/10.1021/ja071274q.
[36] V. Fourmond, P. Infossi, M.-T. Giudici-Orticoni, P. Bertrand, C. Léger, "Two-step" chronoamperometric method for studying the anaerobic inactivation of an oxygen tolerant NiFe hydrogenase, J. Am. Chem. Soc. 132 (13) (2010) 4848–4857, http://dx.doi.org/10.1021/ja910685j.
[37] V. Fourmond, C. Greco, K. Sybirna, C. Baffert, P.-H. Wang, P. Ezanno, M. Montefiori, M. Bruschi, I. Meynial-Salles, P. Soucaille, J. Blumberger, H. Bottin, L. de Gioia, C. Léger, The oxidative inactivation of FeFe hydrogenase reveals the flexibility of the H-cluster, Nat. Chem. 6 (4) (2014) 336–342, http://dx.doi.org/10.1038/nchem.1892.
[38] J.G. Jacques, B. Burlat, P. Arnoux, M. Sabaty, B. Guigliarelli, C. Léger, D. Pignol, V. Fourmond, Kinetics of substrate inhibition of periplasmic nitrate reductase, Biochim. Biophys. Acta 1837 (10) (2014) 1801–1809, http://dx.doi.org/10.1016/j.bbabio.2014.05.357.
[39] V. Fourmond, T. Lautier, C. Baffert, F. Leroux, P.-P. Liebgott, S. Dementin, M. Rousset, P. Arnoux, D. Pignol, I. Meynial-Salles, P. Soucaille, P. Bertrand, C. Léger, Correcting for electrocatalyst desorption or inactivation in chronoamperometry experiments, Anal. Chem. 81 (8) (2009) 2962–2968, http://dx.doi.org/10.1021/ac8025702.
[40] R.C. Bray, S.P. Vincent, D.J. Lowe, R.A. Clegg, P.B. Garland, Electronparamagnetic-resonance studies on the molybdenum of nitrate reductase from *Escherichia coli* K12, Biochem. J. 155 (1) (1976) 201–203 (URL http://www.biochemj.org/bj/155/bj1550201.htm).
[41] J.C. Hilton, C.A. Temple, K.V. Rajagopalan, Re-design of *Rhodobacter sphaeroides* dimethyl sulfoxide reductase. enhancement of adenosine N1-oxide reductase activity, J. Biol. Chem. 274 (13) (1999) 8428–8436, http://dx.doi.org/10.1074/jbc.274.13.8428.
[42] A.F. Bell, X. He, J.P. Ridge, G.R. Hanson, A.G. McEwan, P.J. Tonge, Active site heterogeneity in dimethyl sulfoxide reductase from *Rhodobacter capsulatus* revealed by Raman spectroscopy, Biochemistry 40 (2) (2001) 440–448, http://dx.doi.org/10.1021/bi002065k.
[43] G. George, J. Hilton, C. Temple, R. Prince, K. Rajagopalan, Structure of the molybdenum site of dimethyl sulfoxide reductase, J. Am. Chem. Soc. 121 (6) (1999) 1256–1266, http://dx.doi.org/10.1021/ja982843k.
[44] S. Stoll, A. Schweiger, Easyspin, a comprehensive software package for spectral simulation and analysis in EPR, J. Magn. Reson. 178 (1) (2006) 42–55, http://dx.doi.org/10.1016/j.jmr.2005.08.013.
[45] V. Fourmond, K. Hoke, H.A. Heering, C. Baffert, F. Leroux, P. Bertrand, C. Léger, Soas: a free program to analyze electrochemical data and other one-dimensional signals, Bioelectrochemistry 76 (1–2) (2009) 141–147, http://dx.doi.org/10.1016/j.bioelechem.2009.02.010.
[46] P.T. Boggs, J.R. Donaldson, R.H. Byrd, R.B. Schnabel, Algorithm 676: Odrpack: software for weighted orthogonal distance regression, ACM Trans. Math. Softw. 15 (4) (1989) 348–364, http://dx.doi.org/10.1145/76909.